AGU PUBLICATIONS

JGR

Journal of Geophysical Research: Planets

RESEARCH ARTICLE
10.1002/2016JE005241

Key Points:
- Silicate glasses with different degrees of polymerization are characterized by using vibration spectroscopy
- Raman peak intensities and positions systematically evolve with the degree of polymerization of silicate glasses
- A calibration curve was established to quantify the degree of polymerization of amorphous silicates

Supporting Information:
- Supporting Information S1
- Table S1
- Table S2
- Table S3
- Table S4
- Table S5
- Table S6

Correspondence to:
X. Fu,
fuxh@sdu.edu.cn;
fuxiaohui1985@gmail.com

Citation:
Fu, X., A. Wang, and M. J. Krawczynski (2017), Characterizing amorphous silicates in extraterrestrial materials: Polymerization effects on Raman and mid-IR spectral features of alkali and alkali earth silicate glasses, *J. Geophys. Res. Planets*, *122*, 839–855, doi:10.1002/2016JE005241.

Received 16 DEC 2016
Accepted 8 FEB 2017
Accepted article online 20 MAR 2017
Published online 21 MAY 2017

Characterizing amorphous silicates in extraterrestrial materials: Polymerization effects on Raman and mid-IR spectral features of alkali and alkali earth silicate glasses

Xiaohui Fu[1,2], Alian Wang[3], and Michael J. Krawczynski[3]

[1]Key Laboratory of Lunar and Deep Space Exploration, National Astronomical Observatories, Chinese Academy of Sciences, Beijing, China, [2]Shandong Provincial Key Laboratory of Optical Astronomy and Solar-Terrestrial Environment, Institute of Space Sciences, Shandong University, Weihai, China, [3]Department Earth and Planetary Sciences and McDonnell Center for Space Sciences, Washington University, St. Louis, Missouri, USA

Abstract Amorphous silicates are common in extraterrestrial materials, especially in carbonaceous chondrites of petrologic types 1 and 2. In addition, high percentage of amorphous components and poorly crystalline phyllosilicates were found in the mudstones at Gale Crater by the CheMin instruments on board of Mar Curiosity rover, which illustrates the importance of characterizing amorphous silicates in future planetary surface explorations. The structure of an amorphous silicate can vary in two aspects: the degree of polymerization and the degree of crystallinity. Here we present the first phase study on characterizing synthetic alkali and alkali earth silicate glasses with different degrees of polymerization by using vibration spectroscopy. Compared with crystalline silicates, their Raman and mid-IR spectra show broad spectral peaks but have the similar peak positions. We find that a change in the degree of polymerization of these silicate glasses affects their Raman band positions, especially the ratio of Raman band intensities, as well as the positions of the Christiansen feature and reststrahlen bands in their mid-IR absorbance spectra. Based on these observations, we establish a calibration curve that could enable semiquantification of the polymerization degree of silicate glasses in planetary surface/subsurface materials during future robotic planetary surface exploration missions.

1. Introduction

Amorphous silicates are common in extraterrestrial materials and are a significant component in the fine-grained matrices of CM, CR, CO, and UOC chondrites [*Brearley and Le Guillou*, 2015]. This characteristic has been recognized as a common feature of pristine chondrites [*Brearley and Le Guillou*, 2015].

In addition, amorphous silicates have been detected in Martian meteorites and in Mars surface materials at Gale Crater. In general, since igneous rocks are widely dispersed over the Martian surface (see *McSween* [2015] for a review), volcanic glasses could be a major component in Martian surface materials. The silicate glasses could also be produced from rapid quenching of impact-induced melting of the target rock. Martian impact melts and breccias have been identified from orbit based on their morphology [*Osinski et al*., 2011; *Skok et al*., 2012; *Tornabene et al*., 2010] and in Martian meteorites [*Agee et al*., 2013]. Laboratory studies of Martian nakhlites have revealed phyllosilicate and amorphous silicate in the hydrothermal deposits filling the olivine fractures [*Changela and Bridges*, 2010; *Hicks et al*., 2014; *Ling and Wang*, 2015]. An amorphous, silica-rich phase has also been identified in Martian meteorites ALH84001 [*Cooney et al*., 1999] and NWA 856 [*Leroux and Cordier*, 2006].

Furthermore, a large amount of amorphous phases (likely including amorphous silicates) were found by Chemistry and Mineralogy X-ray diffraction (CheMin) instrument on board the Mars Curiosity rover at Gale Crater on Mars. More than 30% of amorphous component was found in all analyzed samples, and a poorly crystalline smectite was found in mudstone samples, appearing as an elevated background between 15 and 40° in 2θ and a low-angle rise (4–10° in 2θ) in the X-ray diffraction (XRD) patterns, respectively [*Bish et al*., 2013; *Vaniman et al*., 2014; *Grotzinger et al*., 2015]. The structural details of amorphous silicates (and poorly crystalline smectite) are directly linked to the local or regional environmental conditions, e.g., pH, temperature, nature of chemical reaction, and water-to-rock ratio, and ultimately linked to the hydrologic evolution of Mars [*Baker and Strawn*, 2014; *Huertas et al*., 1999].

From orbit, phyllosilicates have been reported on the Martian surface with wide spread occurrences based on analyses of the data from Mars Express/OMEGA and MRO/CRISM [*Bibring et al*., 2007; *Bishop et al*., 2008; *Mustard et al*., 2008; *Poulet et al*., 2005]. This identification is based on the detection via near-infrared spectroscopy of features at 1.4 μm (the first overtone of the O–H stretching modes), 1.9 μm (H–O–H band), and 2.15–2.4 μm (metal–OH bands) features. The discovery of poorly crystalline smectite in mudstones by CheMin inspires a study on the crystallinity of the phyllosilicates found via orbital remote sensing on Mars. Can the structural form of these phyllosilicates be further characterized in global scale? Can the detailed structural features of amorphous silicates be revealed by a suitable technique during surface exploration?

The structure of an amorphous silicate can vary in two aspects: the degree of polymerization and the degree of crystallinity. The former characterizes the basic structural framework of SiO_4 tetrahedra, from ortho-SiO_4, chain-Si_2O_6, and phyllo-Si_4O_{10} to tecto-$(Si,Al)_4O_8$, existing in silicate glasses as well as in crystalline counterparts, which is the target of the current study [*Klein et al*., 2002]. The latter one characterizes the structural distortion (in bond length and bond angle) with respect to a regular crystal in terms of rotational and translational long-range order, which will be the target of the second step of our study [*Klein et al*., 2002].

The degrees of polymerization of silicate glasses/melts affect their chemical, physical, and thermal properties [*Mysen and Richet*, 2005]. The structure of a silicate glass consists of a three-dimensional network of SiO_4 tetrahedra linked by bridging oxygen atoms. The addition of network-modifying cation oxides, such as Na_2O, K_2O, CaO, and MgO, breaks up this network by generating nonbridging oxygen (NBO) atoms. The ratio NBO/T (T = tetrahedrally coordinated cations) is widely used as a measure of the degree of polymerization of silicate crystals/glasses/melts [*Mysen and Richet*, 2005]. A decrease of the NBO/T corresponds to an increase in the bulk polymerization of the silicates. For a nonpolymerized silicate (olivine), the structure consists of isolated TO_4 tetrahedra and none of the oxygen atoms on a TO_4 is linked to another TO_4 (NBO/T = 4). In a fully polymerized silicate (quartz, feldspar, etc.), all TO_4 units linked to each other (NBO/T = 0). The same naming rule applies for crystalline and amorphous silicates as well as for silicate melts [*Klein et al*., 2002].

Amorphous silicates in extraterrestrial materials could form through primary volcanism or secondary processes (e.g., hydrothermal alteration, impact, and radiation damage) [*Rampe et al*., 2014]. The determination of NBO/T ratios could help to constrain the conditions under which these amorphous silicates formed. For instance, the degree of polymerization of volcanic glass could be used for deducing silicate melt properties (e.g., composition, density, and viscosity of melt) and types of volcanic eruption [*Mysen and Richet*, 2005]. In secondary processes, the degree of alteration of a silicate and the conditions under which the secondary silicate formed can affect their structural forms. For example, highly variable degrees of polymerization were found in amorphous silicates in the Tagish Lake (TL) meteorite: transmission electron microscopy (TEM) data revealed some regularly stacked layers with basal spacing suggesting serpentine-saponite-clinochlore [*Noguchi et al*., 2002], whereas XRD indicated a poorly crystalline, fine-grained interlayered saponite-serpentine structure [*Izawa et al*., 2010] and the Raman band intensity ratios further implied a transition from mainly chain-like to phyllosilicate-like amorphous silicates [*Wang and Jolliff*, 2015]. Since TL is one of the most primitive meteorites, the variability in the degrees of polymerization in its amorphous silicates is consistent with a moderate degree of low-temperature alteration in the presence of water [*Zolensky et al*., 2002]. The degree of polymerization of an amorphous silicate increases with the removal of mobile elements during continuous acid leaching [*Burns*, 1993]. The types of poorly crystalline phyllosilicate on Mars are related to their formation conditions. For example, the abundant Fe–Mg smectite clays observed on Mars are likely alteration products of Fe–Mg rich minerals, i.e., olivine, pyroxene, and volcanic glass, formed at a low water-to-rock ratio and low pH. Kaolinite will form after the further leaching of Fe and Mg cations from the smectite, which requires a higher water-to-rock ratio and a different pH [*Greenberger et al*., 2012]. Opaline silica, one type of poorly crystalline high silica phase found on Mars, could be the residual silicates remaining after extensive leaching of mobile elements in environments with high water-to-rock ratios environment [*Horgan and Bell*, 2012] or may be the precipitate from hydrothermal fluids that originally contained high level of SiO_2.

Laser Raman spectroscopy has been extensively used to investigate the structures of silicate glasses/ melts of a variety of chemistries and degrees of polymerization for terrestrial applications [*Brawer and White*, 1975, 1977; *Etchepare*, 1972; *Furukawa and White*, 1991; *Furukawa et al*., 1981; *Matson et al*., 1983; *McKeown et al*., 1984; *McMillan*, 1984a, 1984b; *McMillan and Piriou*, 1983; *McMillan et al*., 1982; *Mercier et al*., 2009; *Mysen*

and Neuville, 1995; *Mysen*, 2003; *Mysen and Toplis*, 2007; *Mysen et al*., 1981, 1982; *Piriou*, 1983; *Seifert et al*., 1981; *Sharma and Simons*, 1981; *Sharma and Matson*, 1984]. Empirical vibrational assignments to the Raman spectral features of these glasses have been frequently determined through comparisons between features in the spectra of the silicate glasses and in those of crystals with similar chemical compositions[e.g., *Brawer and White*, 1975, 1977; *Etchepare*, 1972; *McKeown et al*., 1984; *McMillan et al*., 1982; *Williams et al*., 1989] or based on vibrational calculations for molecular clusters within the glasses [e.g., *Brawer and White*, 1975, 1977; *Furukawa et al*., 1981; *Marinov et al*., 1994; *Zotov et al*., 1996, 1999]. In recent years, Raman spectroscopy has been developed as a quantitative method of determining ferric iron concentration in glasses [*Baert et al*., 2011; *Magnien et al*., 2006; *Di Muro et al*., 2009; *Di Genova et al*., 2016a], the water contents in silicate glasses and minerals [*Thomas*, 2000; *Arredondo and Rossman*, 2002; *Zajacz et al*., 2005; *Behrens et al*., 2006; *Di Muro et al*., 2006; *Thomas et al*., 2008], and the chemical compositions of silicate glasses [e.g., *Di Genova et al*., 2015, 2016b].

Raman spectroscopy was first proposed as a powerful technique for planetary surface exploration in 1995 [*A. Wang et al*., 1995]. Three Raman systems have been selected as the scientific payloads for in situ and/or for standoff sensing in two Mars missions: NASA's Mars 2020 and ESA's 2020 ExoMars rover missions [*Rull et al*., 2014; *Wiens et al*., 2016]. It is thus natural to foresee the use of the accumulated knowledge from above laboratory Raman studies which characterizes the amorphous silicates detected on planetary surfaces. The determination or even semiquantification of the degree of polymerization of an amorphous silicate based solely on its Raman spectrum could help us to understand the amorphous structure and its implications regarding its formation conditions on Mars.

The goal of this study is to characterize amorphous silicates by using vibration spectroscopy. Specifically, this project is composed of three phases: (1) determine how degree of polymerization affects the Raman and infrared spectra of silicate glasses, (2) determine how degree of crystallinity affects the spectra of amorphous phyllosilicates synthesized via controlled hydrothermal treatment, and finally, (3) to use the obtained laboratory results to investigate amorphous materials in extraterrestrial samples.

Our study focuses on silicate glasses with different degrees of polymerization. We synthesized alkali and alkali earth silicate glasses with a range of degrees of polymerizations, i.e., different NBO/T ratios (from 3.55 to 0 for orthosilicate, chain silicate, phyllosilicate, and tectosilicate), and then characterized these silicate glasses by using Raman and mid-IR spectroscopy. Based on these experiments, we developed a calibration curve to semiquantify the NBO/T ratios of silicate glasses, which could be used in Raman spectral studies of extraterrestrial materials in future planetary surface missions.

2. Experiments

2.1. Samples and Sample Preparation

Silicate glasses were synthesized from pure oxides in a range of NBO/T ratios (from 0 to 3.55) following the method of *Mysen et al*. [1980a, 1980b]. The starting material was a homogenized mixture prepared with appropriate quantities of high purity reagent-grade oxides and carbonates, Na_2CO_3, MgO, Al_2O_3, SiO_2, and $CaCO_3$. The oxides were mixed under ethanol and ground in an agate mortar for half an hour. The ground powder (50–60 mg) was mixed with polyvinyl acetate, and then pressed into a pellet of 4 mm in diameter by applying a pressure of 1.2 ton for 2 min. The pellets were attached to Pt loops by fusing them with a torch.

The samples were heated in a Deltech furnace at 1 atm. Depending on the targeted NBO/T and composition of the mixed oxides, the temperature for each experiment fell in a range from 1260 to 1520°C. The experimental durations varied from 2.5 to 5 h. The molten droplet was quenched by dropping the Pt loop into liquid N_2 or deionized water.

The resulting glass bead was crushed, and the pieces were mounted in epoxy and polished for electron microscopy analysis. The homogeneity of the glass was checked via optical and electron microscopy to confirm that it was free of microcrystals.

Two terrestrial volcanic glasses and two types of lunar glass spherule were also investigated in this study. A basaltic glass was collected from an active Kilauea lava flows and quenched in air. The polished Hawaiian glass was examined via electron microscopy. This sample is a homogeneous glass with only a trace amount of albite microcrystals (50–150 μm in length). A sample of rhyolite glass obtained from Glass Mountain,

California was also studied. Microscopic embryonic crystal growths were observed in the BSE images of the polished obsidian. Yellow-brown glass spherules from lunar sample 1,542,734 range in size from 100 to 350 μm. Lunar impact glass beads were selected in lunar regolith sample 6,150,213 from Apollo 16. More mineralogical and chemical details are available in *Gombosi* [2013]. Many of the lunar glass beads show olivine crystallization, but a few small beads are totally crystal free.

2.2. Analytical Methods

2.2.1. Raman and Infrared Spectroscopic Measurements

The Raman spectra of the silicate glasses were collected by using a HoloLab 5000-532 laser Raman spectrometer under a 532 nm laser excitation at Washington University in St. Louis. The Raman shift of each spectrum ranged from 150 to 4300 cm^{-1}. A 20× microscope objective (NA = 0.4) was used to focus the laser beam (6 μm in diameter) onto the glass chips and to collect the Raman scattering produced by each sample. Each measurement was typically conducted with a 20 s exposure time and 2 times accumulations which were coadded to obtain a Raman spectrum with an acceptable signal/noise ratio. Wave number calibration was performed for every 20 measurements by using the Raman peak of a standard crystalline silicon wafer ($520.2 \pm 0.2\ cm^{-1}$). Each Raman spectrum was corrected by using the intensity correction function of HoloLab5000, based on an instrument overall response curve recorded from a National Institute of Standards and Technology certified standard W lamp. For each type of silicate glass sample, over 100 spots of 0.5–1.0 mm in size were analyzed on chips that were free of bubbles and microcrystals.

Mid-IR attenuated total reflectance (ATR) spectra were collected by using a Nicolet Nexus 670 (Thermo Fisher) Fourier transform infrared interferometer (FTIR) spectrometer. A diamond anvil ATR accessory (Golden Gate of Harrick Scientific) was used to perform the ATR measurements. Infrared spectral data were collected to cover the wavelength range of 4000 to 400 cm^{-1} with a 4 cm^{-1} spectral resolution. For each sample, 128 scans (collected over 2.5 min) were averaged to produce each final spectrum. The Nicolet Nexus 670 FTIR spectrometer is purged constantly by using dry-N_2 in order to remove H_2O vapor and CO_2 in system.

2.2.2. Electron-Probe Microanalyses

The chemical compositions of the synthetic silicate glasses were analyzed via quantitative wavelength-dispersive spectroscopy by using the JEOL 8200 electron microprobe at Washington University in St. Louis. The glass sample grains were mounted in epoxy on glass slides. The surfaces were ground/polished with a final grit size of 0.25 μm diamond paste. Beam conditions for EPMA were an accelerating voltage of 15 kV, a beam current of 20 nA, and a defocused beam (10 μm spot size), used to minimize Na migration from the electron beam. The chemical formulas of glasses were calculated from the measured weight percentages of the corresponding oxides.

3. Results and Analysis

3.1. EPMA Results

Table 1 lists the chemical compositions of the five synthetic silicate glasses and four natural glass specimens. The NBO/T parameter for each silicate glass in Table 1 was calculated from the chemical compositions by using the method of *Mysen and Richet* [2005]. In the calculations, Si, Al, and P were treated as network formers, whereas other cations were considered as network modifiers. Backscattered electron images show that the synthetic products are homogenous and microcrystalline-free glasses (Figure 1).

3.2. Raman Spectra of Silicate Glasses

Typical Raman spectra of crystalline silicates and synthetic silicate glasses with similar NBO/T ratios are presented in Figure 2. The spectra obtained in this study are comparable to the results of previous studies on the CaO–MgO–SiO_2 system [*Mysen et al*., 1980a, 1980b, 1982; *Virgo et al*., 1980] and albite glass [*McKeown*, 2005; *McMillan et al*., 1983].

The Raman spectra of the silicate glasses can be clearly divided into three main characteristic spectral regions (Figure 3). The strong and wide spectral envelope (Figure 3) in the high wave number range (800–1200 cm^{-1}, HF) of the spectrum is assigned to the symmetric stretching vibrational mode of the $Si–O_{nonbridging}$ bond in a TO_4 unit [*Furukawa et al*., 1981; *McMillan*, 1984a; *Mysen and Toplis*, 2007; *Neuville et al*., 2014]. This envelope can be deconvolved into four bands which are assigned to symmetric vibrations of the SiO_4 tetrahedra with

Table 1. Chemical Composition of Synthesized and Natural Silicate Glasses

Samples	Analyzed Spots	Chemical Composition (wt %) Na2O	MgO	Al2O3	SiO2	K2O	CaO	MnO	FeO	TiO2	Cr2O3	P2O5	Total	NBO/T
H-003	5	12.137	0.027	20.011	67.790	0.032	0.026						100.024	0.001
J-010	13	0.205	13.004	0.091	67.408	0.168	19.017						99.892	1.28
H-006	5	0.085	24.694	0.050	60.683	0.014	14.290						99.815	1.73
H-005	5	0.137	19.349	0.044	54.510	0.013	25.633						99.686	2.07
H-008	5	0.028	22.250	0.018	40.688	0.007	36.407						99.398	3.55
Obsidian	14	3.382	0.107	13.943	74.579	4.634	0.934	0.024	1.290	0.252	0.001	0.028	99.173	0.01
Hawaii basalt glass	10	2.384	6.129	13.367	50.922	0.477	10.482	0.168	11.536	2.673	0.014	0.262	98.416	0.73
Apollo 15 brown glass		0.118	17.105	7.755	46.122	0.012	8.641	0.274	19.262	0.394	0.628	0.021	100.332	1.66
Apollo16 green glass[a]		0.39	6.82	26.87	44.69	0.06	15.37	0.07	4.99	0.41	0.11	0.14	99.920	0.43

Samples	Calculated Cations Per Formula Unit Na	Mg	Al	Si	K	Ca	Mn	Fe	Ti	Cr	P	O
H-003	1.030	0.002	1.032	2.967	0.002	0.001						8
J-010	0.023	1.107	0.006	3.851	0.012	1.164						10
H-006	0.006	1.272	0.002	2.097	0.001	0.529						6
H-005	0.010	1.045	0.002	1.976	0.001	0.995						6
H-008	0.001	0.864	0.001	1.060	0.000	1.016						4

[a]Data from *Gombosi* [2013].

respectively one, two, three, and four nonbridging oxygen [*McMillan*, 1984a, 1984b; *Merzbacher and White*, 1991; *Mysen et al*., 1980a, 1980b, 1982].

The low wave number range (400–600 cm^{-1}, LF; Figure 3) is a complex mixed stretching and bending mode of the $Si–O_{bridging}–Si$ bridging bond, including four- and six-member ring breathing vibration and the symmetric stretching of the bridging oxygen in T–O–T (T = Si, Al) linkages [e.g., *Matson et al*., 1983; *McMillan*, 1984b; *Mysen et al*., 1980a, 1980b; *Seifert et al*., 1981]. This mode is the dominant feature in the spectra of all of the tetrahedral tectosilicate glasses.

The middle wave number Raman band (MF; Figure 3) near 600–800 cm^{-1} is associated with the $Si–O_{bridging}–Si$ bond that exists in chain-, ring-, and phyllosilicates, in both crystalline and amorphous forms [*McMillan*, 1984a; *Mysen et al*., 1982].

3.3. Mid-infrared Spectra of Silicate Glasses

The mid-IR_ATR spectra of the silicate glasses were acquired in the range 400 to 4000 cm^{-1}. The principle absorption bands of the glasses were found to be concentrated in the midregion (400–1200) cm^{-1} corresponding to the vibration modes of TO_4 units (Figure 4). The broad band near 1000 cm^{-1}, which corresponds to the asymmetric stretching vibrational mode of the TO_4 (T = Si, Al) tetrahedron (reviewed in *King et al*. [2004]), is the most significant feature for each silicate glass with different degrees of polymerization. Another strong band

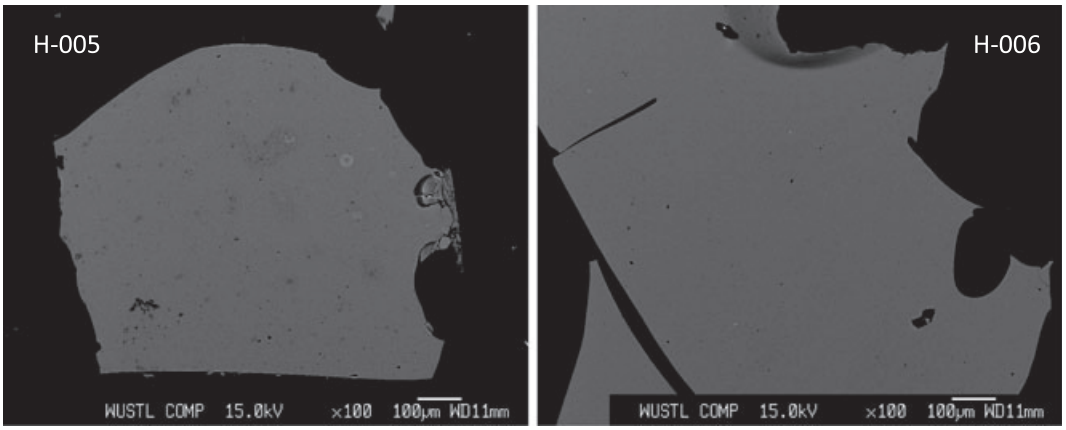

Figure 1. Backscattered electron (BSE) images of silicate glasses H-005 and H-006.

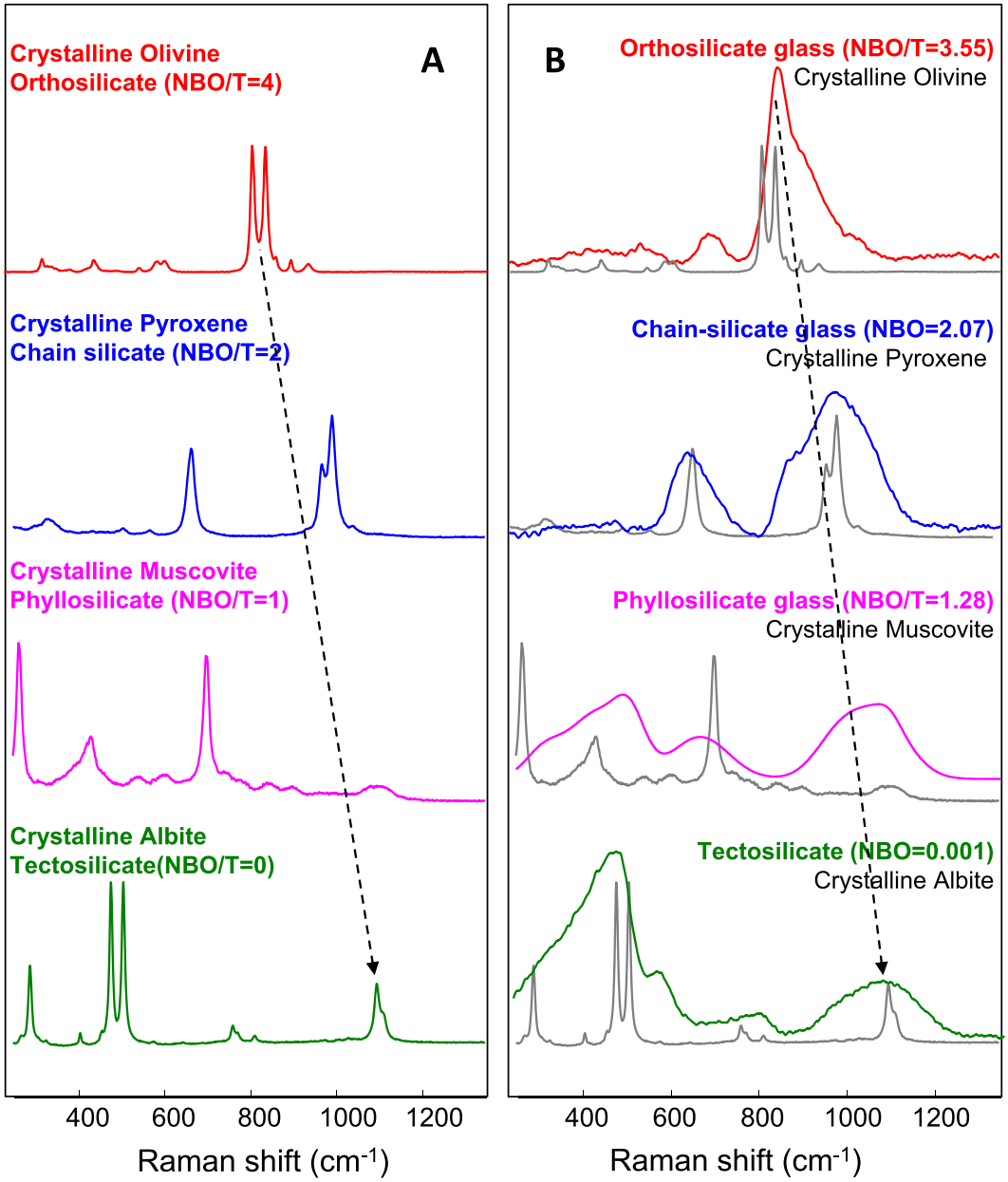

Figure 2. Raman spectra of crystalline silicates and synthesized glasses with similar NBO/T values. (a) Raman spectra of silicate minerals. (b) Comparison of Raman spectra of crystalline silicates and synthesized glasses with similar NBO/T values. (left and right). The dashed lines with arrows show Raman peaks shift win silicates with increasing NBO/T. The intensity of each spectrum was rescaled for the purpose of spectral shape comparison. In general, the Raman scattering intensity from glasses is 1–2 orders of magnitude weaker than that from crystalline materials of similar compositions.

at 400–550 cm^{-1} is due to the O–Si–O deformation or bending modes [*Dalby and King*, 2006]. The weak 730 cm^{-1} band is assigned to the symmetric stretching of the Si–O–Si band [*Dalby and King*, 2006].

4. Discussion

4.1. Comparison of the Raman Spectra of Silicate Crystals and Glasses

The Raman spectra of silicate glasses have very similar peak positions to those of crystalline silicates with the similar NBO/T. Figure 2a shows the Raman spectra of some typical ortho-, chain-, phyllo- and tectosilicates, and Figure 2b compares the Raman spectra of crystalline and glassy silicates with the similar NBO/T.

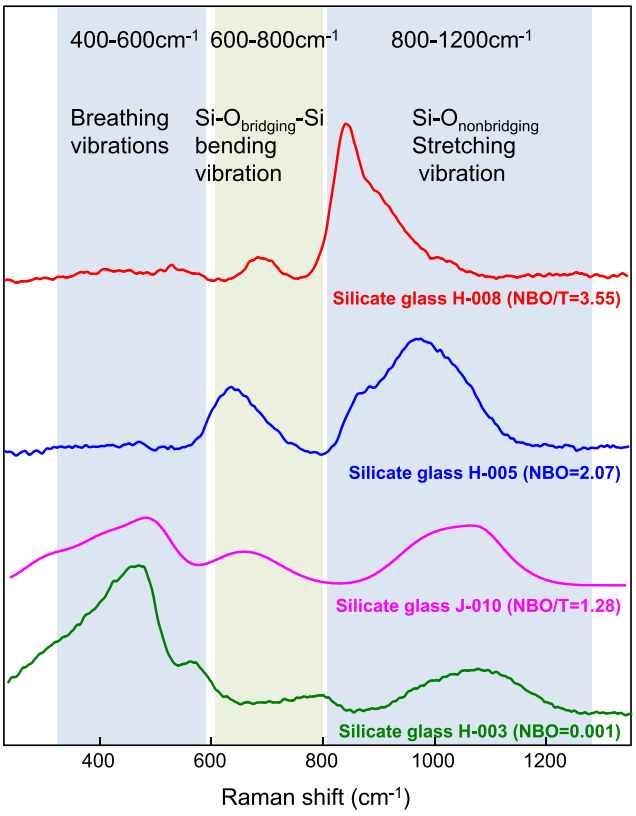

Figure 3. Raman spectra of synthetic silicate glasses (NBO/T ratios ranging from 0 to 3.55) and Raman band assignments.

The dominant features in the Raman spectrum of olivine (NBO/T = 4) are two strong peaks in the 800–860 cm^{-1} region produced by the symmetric stretching vibrations of the SiO_4 group in the olivine structure [*A. Wang et al.*, 1995]. Silicate glass H-008 (NBO/T = 3.55) also exhibits a strong Raman peak centered at 860 cm^{-1} (Figure 2b, first set of spectra). Another Raman band observed for this glass in the region 650–750 cm^{-1}, associated with Si–$O_{bridging}$–Si bending vibration, is very weak since its structure consists mainly of isolated SiO_4 tetrahedral with four nonbridging oxygen, connected to alkaline and alkaline earth cations but not connected to another Si [e.g., *McMillan*, 1984b].

Silicates with a chain structure, such as pyroxene (NBO/T = 2), have a strong double peak near 1000 cm^{-1} and a strong peak near 670 cm^{-1} [*Wang et al.*, 2001]. Two broad bands are also found in the Raman spectrum of a silicate glass H-005 (NBO/T = 2.07), with the central positions of the two bands matching very well with the sharp peaks of pyroxene (Figure 2b, second set of the spectra).

The Raman spectra of most crystalline phyllosilicates (NBO/T = 1) are composed of three spectral groups: $<$600 cm^{-1}, 800–600 cm^{-1}, and 1150–800 cm^{-1} [*Wang et al.*, 2015]. These groups correspond well (Figure 2b, third set of spectra) to the three main wide envelopes of silicate glass J-010 (NBO/T = 1.28).

The Raman spectra of albite (NBO/T = 0) show the strongest peaks between 350 and 550 cm^{-1}, which can be assigned to vibrational modes that are dominated by four-member tetrahedral ring deformations [*Freeman et al.*, 2008]. Despite some loss of spectral details, the broad bands at wave numbers below 600 cm^{-1} are also the prominent feature in albitic glass H-003 (NBO/T = 0.001).

Silicate glasses share the similar central peak positions with the crystalline polymorphs that exhibit similar polymerization characteristics. This suggests that the local structures in silicate with the same NBO/T are similar, regardless of whether they are crystalline or amorphous phase.

For both crystalline and glassy silicates, the positions of the Si–$O_{nonbridging}$ peaks shift upward and the center of Si–$O_{bridging}$–Si peaks shift downward with an increasing degree of polymerization (as indicated by a short dashed line in Figures 2a and 2b). It has been found that in crystalline silicates, the Raman peak positions in the 850–1100 cm^{-1} spectra region gradually move toward higher wave numbers with an increasing of degree of polymerization [*Wang and Jolliff*, 2015]. Silicate glasses display the same trend in their band shifts.

Silicate glasses contain coexisting structural species. These species, referred to as SiO_4, $-SiO_3$, $=SiO_2$, and $\equiv$SiO groups, give rise to four main Raman bands near 850 cm^{-1} and 900 cm^{-1} and at 950–1000 cm^{-1} and 1050–1100 cm^{-1}. Their relative abundance is a function of the silicate's degree of polymerization [*McMillan*, 1984b]. Therefore, the center of Raman band near 1000 cm^{-1} shifts upward to higher frequency as a silicate glass becomes more polymerized as along with the decrease in NBO/T and vice versa.

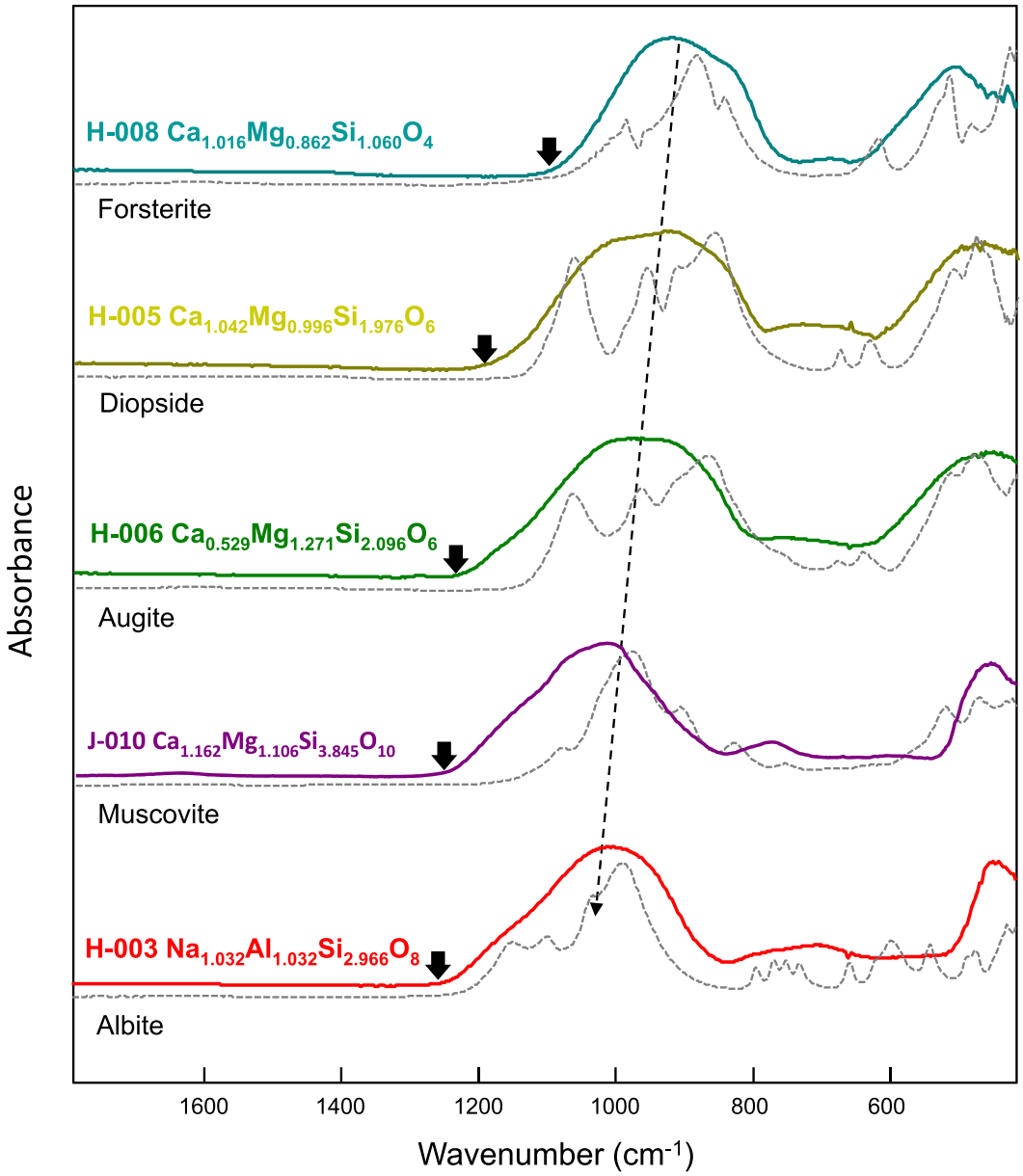

Figure 4. Mid-infrared (MIR) absorbance spectra of crystalline silicates and synthesized glasses with similar NBO/T values. The gray dashed lines are the MIR spectra of silicate minerals, while the color solid lines are the spectra of synthetic silicate glasses. The arrows show the position of Christiansen feature. The dashed line shows the reststrahlen band shift with increasing NBO/T.

Another Raman band at 650–750 cm^{-1}, assigned to $Si–O_{bridging}–Si$ bending vibrations, appears at high intensities in silicate glasses H-005, H-006, and J-010 (NBO/T = 2.07, 1.73, 1.28). For the CaO–Mg–SiO_2 system, this band shifts toward lower frequencies from 700 cm^{-1} to 620 cm^{-1} with an increasing degree of polymerization. This shift band center is consistent with previous studies on silicate glasses [*McMillan*, 1984b]. Notably, this band disappeared in the Raman spectrum of albite glass H-003. The intermediate band (700–800 cm^{-1}) in albite glass is attributed to intratetrahedral and intertetrahedral deformation modes involving significant tetrahedral cation motions as well as AlO_4 stretching vibrations [*Daniel et al.*, 1995].

The Raman band intensities in the LF and HF regions are strongly correlated with the degree of polymerization of silicate glasses. A gradual reduction in intensity of the Raman bands in the spectral region of 850–1100 cm^{-1} with an increasing degree of polymerization has been observed in crystalline silicates. We find

in this study that a similar trend holds for silicate glasses. A Raman band at 400–600 cm^{-1} appears for all silicate structural units except orthosilicate glass (H-008, NBO/T = 3.55) [*McMillan and Piriou*, 1983]. The intensities of the Raman bands in this range increase systematically with the degree of polymerization for both crystalline and glassy silicates. Therefore, the band intensity ratios, expressed as area ratios of the form A_{LF}/A_{HF}, can be correlated with the degrees of polymerization of silicate glasses. This method is described further in section 4.3.

4.2. Comparison of the MIR Spectra of Silicate Crystals and Glasses

Silicate glasses have broad mid-IR spectral bands, but the central band positions are similar to those of crystalline silicates (Figure 4). Laboratory studies and theoretical calculations of the MIR spectra of silicate minerals reveal two diagnostic spectral features: the Christiansen feature (CF) and the Reststrahlen bands (RBs).

The CF occurs near 8 μm (1250 cm^{-1}), manifesting as a minimum in reflectance or a maximum in emission (marked with a black arrow for each spectrum in Figure 4). The position of the Christiansen feature is an indicator of silicate mineral composition, but it does not vary as a function of grain size, crystal orientation, or crystallinity [*Moroz et al*., 2009; *Salisbury and Wald*, 1992]. Through the variation in silicate composition, CF can also be related to a silicate's degree of polymerization. It occurs at higher wave numbers for tectosilicates with framework structures and at lower wave numbers for orthosilicates with isolated Si tetrahedral units (Figure 4). This spectral feature is also observed in the spectra of silicate glasses synthesized in this study with different NBO/T ratios, as a minimum in the absorbance spectrum (see arrows in Figure 4). The CF position progressively shifts upward to higher wave numbers with an increasing degree of polymerization.

Reststrahlen bands (RBs) are the results of strong fundamental molecular vibrations. For silicates, RBs appear as a broad band at 8.5–12 μm (~800–1100 cm^{-1}) due to the asymmetric stretching vibrations of TO_4 units and a feature near 20–25 μm (400–500 cm^{-1}) due to bending vibrations [*Salisbury et al*., 1991]. The RB positions of silicate glasses generally match with those of crystalline phases with similar degree of polymerization. The position of the Reststrahlen band near 1000 cm^{-1} gradually migrates to lower wave numbers as a glass becomes depolymerized. This is the same as the band downshift observed for crystalline silicates by *Launer* [1952]. This suggests that the degree of polymerization affects the infrared spectra features of silicate glasses, as also shown by *Dalby and King* [2006].

The spectral details of the synthetic glasses are markedly distinct from those of the crystalline silicates. All sharp bands observed in the MIR spectra of the crystalline minerals are totally absent in the spectra of their glass analogs. This absence of infrared band splitting in the silicate glasses indicates structural differences between glassy and crystalline polymorphs. Crystalline phases possess long-range order, with well-defined Si–O bond angles and lengths for all TO_4 units. Differences in site symmetry of the TO_4 units generate the vibrational fine structure. By contrast, silicate glasses have only short-range order. The lack of the long-range order results in a broader distribution of Si–O bond angles and lengths when all TO_4 units are considered. These distributions result in broad and smooth infrared spectral features and give rise to the amorphous band structure of silicate glasses [*Speck et al*., 2011].

4.3. Semiquantifying the Degree of Polymerization of Silicate Glasses

Molecular spectroscopic studies of the extraterrestrial samples have played a key role in understanding the properties of planetary objects (planets, satellites, asteroids, and comets) in the solar system and the nature of the building blocks during various periods of solar system formation and stellar evolution. In addition to the compositions of silicate minerals, information on their structural characteristics, especially for amorphous silicates, can be extremely useful in establishing constraints on the geological conditions that prevailed during their formation. Raman spectroscopy is playing an increasingly important role in the laboratory study of extraterrestrial materials and will be a powerful tool for planetary surface missions.

In the laboratory, the structures of silicate melts/glasses have been determined by using a variety of techniques, such as Raman spectroscopy, TEM, neutron diffraction, nuclear magnetic resonance spectroscopy, and X-ray absorption near edge spectroscopy [*Henderson*, 2005]. Among them, Raman spectroscopy appears to be the only effective and practicable method that might offer the ability to perform further structural characterization of amorphous silicates during a robotic planetary surface exploration.

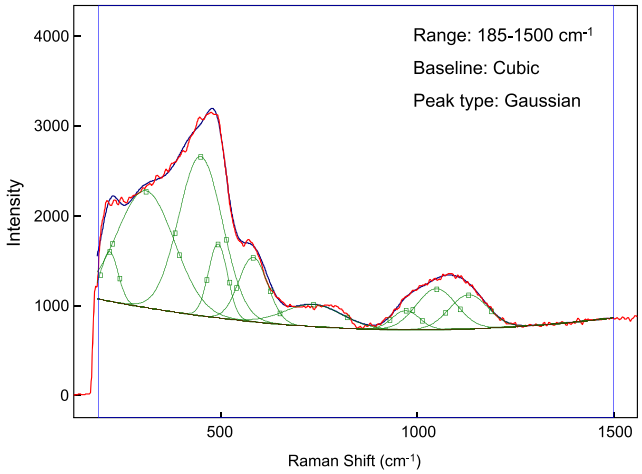

Figure 5. An example of Raman spectrum curve fitting. The red and dark-blue lines represent the origin and fitted Raman spectrum. The green lines are Gaussian peaks. The blue box shows Raman spectrum range of curve fitting.

Based on our observations, we find that the Raman band intensity ratios, expressed as area ratios in the form $A_{(LF+MF)}/A_{HF}$, are correlated with the degrees of polymerization of silicate glasses. This ratio reaches its maximum for crystalline and amorphous orthosilicates and is at its minimum for tectosilicates and silicate glasses with NBO/T ~ 0. Here we develop a calibration curve relating the Raman band area ratio to the degree of polymerizations for amorphous silicates (NBO/T). This method can be used to quickly quantify or semiquantify the structural characteristics of silicate glasses/melts in future planetary missions.

4.3.1. Raman Band Area Extraction and Curve Fitting

Curve fitting was performed to obtain the Raman band areas of the synthetic silicates glasses. In this study, we used the integral band area instead of the intensities of individual Raman bands. We treated each spectral envelope as a superposition of several Raman bands with Gaussian line shapes. For each type of silicate glass, 40 representative Raman spectra from different microspots were selected for spectral curve fitting. Before performing curve fitting, all the acquired spectra were corrected for the wavelength of the excitation laser source and temperature dependence of the Raman intensity according to *Long* [1977]. Curve fitting was performed by using the program package GRAMS/AI 8.0 software suite in three consecutive steps: (1) spectral range fixing, (2) baseline removal, and (3) Raman spectral envelope deconvolution. An example of Raman spectrum curve fitting is shown in Figure 5.

First we fixed the range of the Raman spectrum to the characteristic wave number interval that is characteristic for a specific silicate glass. This is helpful for comparing the Raman curve fitting results with other studies. The major Raman bands of silicate glass H-008 lie in the range 600–1250 cm^{-1}. Thus, we reduced the spectrum of H-008 to this wave number interval. For silicate glass H-003 with a strong band in the LF region, the spectral region we chose was 185 to 1500 cm^{-1}. The other three glasses (H-005, H-006, and J-010) were fitted over the spectral range of 250 to 1600 cm^{-1}.

One issue is how to constrain the baseline in the low wave number range, particularly for highly polymerized glasses, because of the overlap of various bands in the range 100–600 cm^{-1}. In the current study, we set the minimum between the MF and HF peaks (about 790–850 cm^{-1}) as a base point through which baseline was required to pass. The spectral baseline was calculated by fitting a third-order polynomial function in the spectral region of 1250–1800 cm^{-1} and extrapolated it to lower wave numbers, and finally, this fitted baseline was subtracting it from the entire spectrum. The spectrum in this region (1250–1800 cm^{-1}) exhibits no Raman peaks for any silicate species. Therefore, this region was used to determine the baseline for each spectrum. This is a practical way to estimate the background of each Raman spectrum with a high reproducibility, and this method can be applied for the baseline correction for the Raman spectrum of any amorphous silicate.

The number of Gaussian subpeaks to be used in the curve fitting of each spectral envelope (HF, MF, and LF) was chosen in the following way: we started with a minimum number of Gaussian bands and then added bands until no further improvement in the residual error could be obtained. The spectral envelope between 850 and 1250 cm^{-1} was usually deconvolved into three or four Gaussian bands, as generated by $Si–O_{nonbridging}$ vibrations. The spectral envelope near 700 cm^{-1} was usually fitted with one or two Gaussian bands. The number of Gaussian bands in the LF regions differed for five glasses: 0 for H-008 and H-006, 1 for H-005, 3 for J-010, and 5 for H-003. The results of this method of selecting the number of Gaussian bands for the HF, MF, and LF spectral envelopes are generally consistent with the assignments of the corresponding Raman bands.

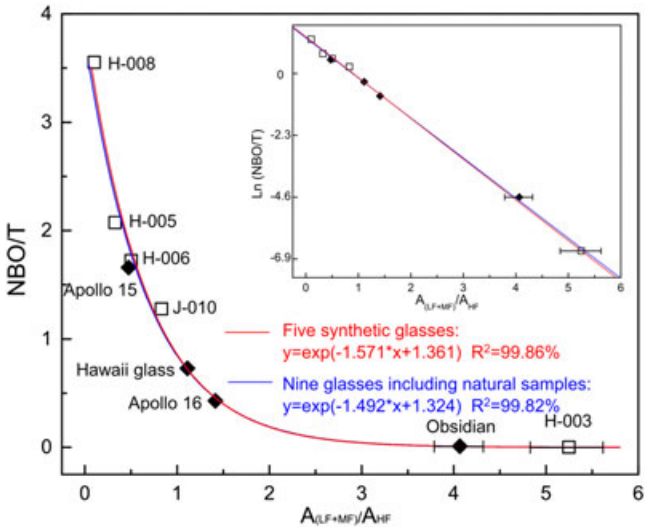

Figure 6. The relationship between NBO/T and Raman band area ratio $A_{(LF+MF)}/A_{(HF)}$. The open boxes are synthesized silicate glasses, and the solid diamonds are natural silicate glasses. The red and blue curves are regression lines for 5 sample points and 9 points, respectively. The error bars of Raman band ratios are smaller than the symbols, if not showing in the figure. The inset plot shows the linear relationship of Raman data with *y* axis as the natural logarithm of NBO/T.

We did not choose the Gaussian curve widths and positions during curve fitting. In the GRAMS/AI program, we set only the number of Gaussians. The Levenberg-Marquardt algorithm was then applied to iteratively adjust the width and height of each Gaussian to minimize the residual error between the modeled and the measured Raman spectra.

4.3.2. Establishing the Calibration Curve

Figure 6 shows the evolution of NBO/T as a function of the Raman band area ratios $A_{(LF+MF)}/A_{HF}$ and the ratio variations among the five silicate glasses (open square symbols). As previously discussed, it is well known that the relative intensity of the LF and HF bands of a silicate glass decreases as the glass becomes more depolymerized [*Behrens et al.*, 2006; *Di Muro et al.*, 2006; *Mercier et al.*, 2009]. Here we establish an equation relating the Raman band ratio $A_{(LF+MF)}/A_{HF}$ to NBO/T for five synthetic glasses. The Raman band ratio exhibits a linear relationship with ln(NBO/T) in Figure 6 (insert). This curve (red color curve) was fitted with an exponential function:

$$\ln(\mathrm{NBO/T}) = -1.517^{*}\times + 1.361 \quad \text{with an } R^2 = 99.86\%,\ n = 5 \tag{1}$$

To validate this calibration curve, we investigated four natural silicate glasses (solid black diamond symbols in Figure 6) with very different but known NBO/T values (Table 1). They were all found to fall on the red curve, with the data from the Apollo 15 brown glass bead showing a slightly deviation. These findings demonstrate the applicability of our calibration curve for quantifying the NBO/T ratios of silicate glasses.

If we include all data from four natural glasses into the determination of a calibration curve, then the equation (blue curve in Figure 6) becomes

$$\ln(\mathrm{NBO/T}) = -1.492^{*}\times + 1.324 \quad \text{with an } R^2 = 99.82\%,\ n = 9 \tag{2}$$

In Figure 6, the difference between the red curved obtained from the regression analysis of the 5 points associated with the synthetic glasses (equation (1)) and the blue curve based on the data from all tested silicate glass data (equation (2)) is negligible. The latter regression (equation (2)) is recommended for future NBO/T quantification based on Raman band area ratios because of the inclusion of data from natural silicate glasses. Using this calibration curve, the degrees of polymerization of amorphous silicates in extraterrestrial materials can be extracted based upon the Raman spectra acquired during data analysis for a robotic investigation of rock on a planetary surface (Mars2020 and ExoMars).

4.3.3. Error Source Analysis

There are several sources of error in equation (2): (1) the intrinsic error of the Raman measurements, (2) the heterogeneity of each specimen, and (3) the curve fitting of the Raman band.

Regarding point (1), all of the Raman spectra of the silicate glasses were acquired under the same conditions by using the same instrument. We also verified that an increase in the accumulation time did not appreciably

increase the precision of Raman band ratio. Regarding point (2), the Raman spectrum of each type of silicate glass was collected from several chips of a crushed synthetic glass bead. Furthermore, only homogeneous chips free of bubbles and microcrystals were analyzed. Both of these measures were intended to limit the importance of heterogeneity effects.

Several sources of error may also arise in the curve-fitting procedures, such as the use of an incorrect baseline or the presence of small, undetected small peaks. The standard error on the Raman band area is expressed as the standard deviation (SD) of the difference between the raw spectrum and the fitted curve. The SD values given in Table 2 and the error bars (Figure 6) for Raman band area ratios $A_{(LF+MF)}/A_{(HF)}$ were determined via error propagation from the standard error on the curve-fitted Raman band areas.

Natural silicate glasses/melts may contain microcrystals because of devitrification and recrystallization of the glasses. Small skeletal crystals of olivine were also observed in the green glass beads from Apollo 1,542,734. The presence of such microcrystals results in sharp peaks overlaid on the broad and smooth Raman spectra of silicate glasses. This could pose a problem for the curve fitting of the Raman spectrum and precise peak area extraction. These sharp peaks could therefore affect the determination of NBO/T by using the calibration curve. More work will be needed in the future to establish a quantitative method for subtracting the contributions of microcrystals from Raman spectra of silicate glasses.

Compared with the other synthetic glasses, the Raman band area ratios of H-003 show a higher uncertainty; the same is also true of the natural silica-rich obsidian (Figure 6). Aside from the sample heterogeneity, the spectral curve fitting, especially baseline removal, is the main source of the uncertainty for H-003. A small variation in the baseline could result in a change to Raman band area. Therefore, polymerized silicate glasses with one or more strong peaks below 600 cm^{-1} could be subject to higher uncertainties in the Raman band area ratio.

4.3.4. The Applicability of the Calibration Curve

This study is based on synthetic alkali and alkaline earth silicate glasses with simple chemical compositions. All synthetic silicate glasses are free of iron and titanium. The Al, Ti, and Fe that are present in natural silicate glasses/melts complicate their structures and Raman spectra. This may lead to errors when our calibration curve is applied to determine the NBO/T ratios of natural amorphous silicates.

In the structure of a silicate glass/melt, Al, Ti, and Fe can act as both network formers and network modifiers. Charge compensation by an alkali cation allows Al^{3+} and Fe^{3+} to substitute for Si^{4+} as a network former [*Mysen et al*., 1982]. It has been found that the 800–1200 cm^{-1} envelope shifts to lower frequencies with increasing Al/(Al + Si) [*Neuville and Mysen*, 1996], and the substitution of Si^{4+} by Al^{3+} is expected to cause the scattering cross section in the HF region to increase [*Di Muro et al*., 2006 and references therein]. As a result, the $A_{(LF+MF)}/A_{HF}$ ratio of SiO_2 glass is higher than that of albite glass. The variation in the Raman spectral topology depends on both Al^{3+} substitution in tetrahedral coordination and the metal cation abundance related to charge balance [*Rossano and Mysen*, 2012].

Ti atoms exist in silicate glasses/melts with a range of coordination numbers from four to six and can appear at least three different structural positions depending on the TiO_2 concentration, temperature, and pressure [*Mysen and Neuville*, 1995]. For low Ti contents, Ti^{4+} acts as a network-modifying cation. In the $CaO–SiO_2$ glasses with a Ti content of $<$6 cat % [*Alberto et al*., 1995] and $Na_2O–SiO_2$ glasses with a TiO_2 content of less than 1 mol [*Mysen and Neuville*, 1995], no obvious Raman band shift or intensity modification is observed.

The effects of iron on the Raman spectra of silicate glasses are even more complicated. Changes involving iron and its oxidation state (Fe^{3+}/Fe_{tot}) can induce appreciable variations in the structure and properties of a glass [*Lange and Carmichael*, 1989], as well as its Raman spectra [*Di Genova et al*., 2016a and references therein]. *Sharma et al*. [1997] found that the substitution of Fe^{3+} in tetrahedral coordination results in a Raman band at 965 cm^{-1}. *Magnien et al*. [2006] observed increases in the intensity f the Raman bands at both 400–700 cm^{-1} and 800–1200 cm^{-1} in the $SiO_2–CaO–MgO–Na_2O–FeO$ system with increasing Fe^{3+}/Fe_{tot}. Moreover, the latter envelope, which is associated with symmetric T–O stretching (T = Si^{4+}, Al^{3+}, Fe^{3+}), is more sensitive to the iron redox state [*Mysen et al*., 1980a, 1980b; *Z. Wang et al*., 1995], shifting to lower wave numbers with increasing Fe^{3+}/Fe_{tot}. Based on these observations, Raman spectroscopy has been used to determine changes in the redox ratio by *Di Muro et al*. [2009] and *Di Genova et al*. [2016a].

Table 2. Raman Band Area Ratios of Synthesized Silicate Glasses

	H-008	H-005	H-006	J-010	H-003	H-006	J-010	H-003
NBO/T	3.55	2.07	1.72	1.28	0.001	1.72	1.28	0.001
Area Ratio	0.101 ± 0.020	0.327 ± 0.011	0.501 ± 0.053	0.829 ± 0.055	5.247 ± 0.458	0.154 ± 0.075	0.411 ± 0.045	4.961 ± 0.445
	$A_{(LF+MF)}/A_{HF}$					A_{LF}/A_{HF}		
1	0.080	0.336	0.559	0.848	5.507	0.169	0.436	5.325
2	0.098	0.329	0.459	0.836	5.316	0.077	0.388	4.929
3	0.078	0.331	0.561	0.756	5.927	0.190	0.396	5.384
4	0.116	0.313	0.501	0.721	4.880	0.139	0.357	4.483
5	0.129	0.324	0.478	0.686	5.355	0.095	0.296	5.226
6	0.094	0.321	0.472	0.824	5.999	0.091	0.412	5.643
7	0.097	0.311	0.471	0.885	5.599	0.107	0.463	5.491
8	0.102	0.336	0.455	0.885	5.220	0.125	0.429	4.927
9	0.075	0.312	0.504	0.805	5.773	0.129	0.368	5.570
10	0.105	0.318	0.488	0.870	5.664	0.127	0.451	5.265
11	0.092	0.319	0.476	0.826	4.757	0.109	0.416	4.313
12	0.078	0.303	0.479	0.783	5.512	0.119	0.388	4.964
13	0.081	0.309	0.491	0.781	4.953	0.116	0.372	4.666
14	0.075	0.307	0.475	0.883	5.556	0.171	0.454	5.446
15	0.081	0.342	0.504	0.844	5.384	0.211	0.428	4.724
16	0.109	0.327	0.542	0.801	5.645	0.214	0.407	5.259
17	0.086	0.330	0.593	0.800	5.969	0.254	0.404	5.563
18	0.086	0.302	0.556	0.818	5.401	0.214	0.391	5.388
19	0.091	0.318	0.602	0.851	5.546	0.267	0.419	5.213
20	0.089	0.322	0.446	0.794	4.998	0.151	0.379	4.615
21	0.103	0.334	0.424	0.804	5.351	0.108	0.387	5.242
22	0.074	0.340	0.452	0.808	4.579	0.159	0.392	4.457
23	0.098	0.330	0.514	0.883	4.165	0.240	0.443	3.954
24	0.100	0.334	0.549	0.873	5.868	0.038	0.445	5.558
25	0.132	0.337	0.618	0.806	5.209	0.335	0.398	5.033
26	0.109	0.338	0.548	0.845	5.118	0.269	0.419	4.772
27	0.107	0.323	0.670	0.796	4.699	0.334	0.398	4.397
28	0.105	0.332	0.468	0.797	4.849	0.144	0.373	4.482
29	0.126	0.334	0.461	0.775	4.288	0.113	0.352	4.120
30	0.135	0.335	0.519	0.778	4.928	0.048	0.343	4.549
31	0.175	0.349	0.526	0.791	5.142	0.177	0.346	5.014
32	0.099	0.337	0.511	0.904	5.100	0.197	0.492	4.781
33	0.109	0.333	0.600	0.916	5.383	0.261	0.467	5.079
34	0.118	0.336	0.466	0.871	5.471	0.111	0.440	5.039
35	0.102	0.324	0.470	0.902	4.417	0.103	0.506	4.309
36	0.089	0.338	0.475	0.824	5.216	0.095	0.397	5.064
37	0.086	0.337	0.449	0.797	5.062	0.082	0.397	4.862
38	0.105	0.327	0.430	0.823	5.634	0.054	0.407	5.385
39	0.123	0.328	0.453	0.934	5.828	0.066	0.491	5.453
40	0.090	0.340	0.519	0.954	4.624	0.155	0.496	4.501

Natural silicate melts/glasses have complicated chemical compositions. Al, Ti, and Fe can be major cations in these materials. The influences of individual cations on the Raman spectra of silicate glasses have been investigated previously. However, it is difficult to use the available knowledge to determine the combined effects of these elements. In this study, we compared the relationships between the Raman band area ratio and the NBO/T ratio determined based on synthetic silicate glasses and natural silicate glasses with more complicate chemical features: Hawaii basalt glass, Apollo 15 brown glass, and Apollo 15 green glass contain FeO at levels of 11.5, 19.3, and 5 wt%; Hawaii basalt glass contains 2.7 wt % of TiO_2, whereas the other three glasses contain 0.25–0.41 wt % TiO_2; the content of Al_2O_3 content in the four natural glasses varies from 7.8 to 26.9 wt % (Table 1).

Figure 6 shows the regression curves of $A_{(LF+MF)}/A_{HF}$ versus NBO/T. The red curve is based on the five synthetic alkali and alkaline earth silicate glasses. Note that the Raman data from the four natural silicate glasses (filled diamond symbols) all fall on this red curve. These natural silicate glass samples contain varying amounts of Al, Ti, and Fe as well as Fe^{3+}/Fe_{tot}. Despite these chemical distinctions, the red curve essentially

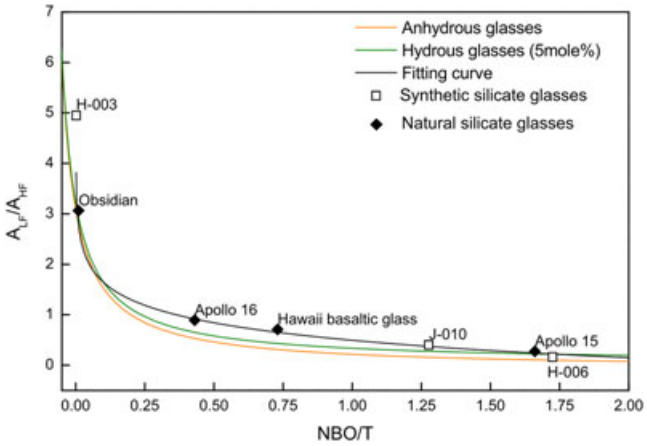

Figure 7. Variation of Raman band ratios A_{LF}/A_{HF} with NBO/T in silicate glasses. The black and blue lines represent the empirical equations between A_{LF}/A_{HF} ratio and NBO/T in anhydrous and hydrous silicate glasses, copied from *Mercier et al*. [2009]. The red line is the regression curve based on the data of silicate (synthetic and natural) glasses in this study, expressed as $A_{LF}/A_{HF} = -0.547 * \ln(\text{NBO/T}) + 0.510$.

overlaps with the blue regression curve, which is based on the five synthetic glasses and the four natural glasses.

Mercier et al. [2009] constructed an empirical calibration relating the A_{LF}/A_{HF} ratio to NBO/T for anhydrous and hydrous glasses with 5 mol % water. The glasses tested by these authors contained different amounts of Al, Ti, and Fe and exhibited various iron oxidation states. Figure 7 shows a comparison of our regression curve with those of *Mercier et al*. [2009]. The data from our synthetic and natural silicate glasses (black diamonds in Figure 7) follow the same general trend observed for the dry and hydrous glasses (black and blue lines) of *Mercier et al*. [2009], with slightly higher A_{LF}/A_{HF} values at higher NBO/T values.

Following the above discussions, it is clear that some chemical features (Al, Ti, and Fe and its oxidation state) can affect the positions and intensities of Raman bands. However, since we consider only the ratios of the integrated Raman band areas (A_{LF}/A_{HF} or $A_{(LF+MF)}/A_{HF}$) in this study, the effects of other Raman spectral features on these peak area ratios are not obvious. Therefore, the calibration curve developed in this study can be applied for the semiquantification of the degrees of polymerization of silicate glasses, apparently including Na-, Mg-, Al-, Fe-, and Ti-containing glasses.

In addition, our intension is to use the calibration curve developed in this study to evaluate the degrees of polymerization of silicate glasses found during future surface missions to Mars. Semiquantification of the degree of polymerization based on Raman data collected on the surface of Mars will provide first-hand structure information of amorphous silicates present in the planetary surface. Al, Ti, and Fe may result in slight deviations between the NBO/T value calculated from the Raman band area ratio and true NBO/T value, but these deviations are within the limits of the systematic error of the calibration curve.

4.3.5. Future Application on Planetary Sciences

Three Raman spectrometers are being developed for surface exploration missions on Mars (e.g., ESA ExoMars 2020 rover mission and NASA Mars 2020). They are part of the core payloads for mineralogy and geochemistry of those rover missions.

Abundant amorphous silicates have been found on Mars, either as sedimentary deposits, volcanic products, or impact-related deposits [*Cannon and Mustard*, 2015; *Horgan and Bell*, 2012]. The calibration curve we present here can be directly applied to semiquantify the degrees of polymerization of silicate glasses found by future Mars rovers.

Based on the structure information revealed by Raman data analyses, it should be possible to make inferences regarding the formation process of amorphous silicates, e.g., (1) details about volcanic lava (density and viscosity), types of volcanic eruption, and the cooling processes [*Mysen and Richet*, 2005]; (2) the duration of acid leaching in a hydrothermal alteration environment; and (3) the restoration of the original crystalline silicate.

To ensure proper use of our calibration curve, we offer several suggestions. First, multiple Raman spectra of amorphous silicate should be acquired. Second, the Raman spectra should be corrected for the wavelength of the excitation laser source, instrumental spectral response, and temperature dependence of the Raman intensity according to *Long* [1977]. Third, the curve fitting of the Raman spectrum should follow the three steps and guiding principles presented in section 4.3.1. Fourth, it should be kept in mind that the calibration curve is developed based on the alkali and alkaline earth silicate glasses; we advise greater cautions when

using this curve to quantify the NBO/T ratios of silicate glasses with more complicated chemistries. In the third phase of our study, we will collect Raman spectra from additional silicate glasses/melts and add these data to Figure 6, which could improve the applicability of the calibration curve.

5. Conclusions

This study focused on the characterization of alkali and alkaline earth silicate glasses with different degrees of polymerization using vibration spectroscopy. Compared with crystalline silicates with similar degrees of polymerization, the vibrational spectra of amorphous silicates have the same overall shapes as those of their crystalline analogs. However, they lack the fine structure and narrow bandwidths that are present in the crystalline analogs. The Raman and mid-IR spectra of synthetic glasses are characterized by broad spectral bands with similar central positions to that of their crystalline counterparts. The position of the Raman band near 1000 cm^{-1} shifts upward to higher wave numbers with an increasing degree of polymerization, whereas the 600 cm^{-1} peak moves toward lower wave numbers. When silicate glasses become more polymerized, there is a weakening of the Raman band near 1000 cm^{-1} (Si–$O_{nonbridging}$ stretching mode) and a strengthening of the broad Raman bands near 500 cm^{-1} and 700 cm^{-1} (Si–$O_{bridging}$–Si vibrations). The systematic variation in the Raman band intensities is strongly correlated with the degree of polymerization. In the MIR absorbance spectra, the positions of the fundamental absorption bands gradually migrate toward lower wave numbers with the depolymerization of the glasses. All of the sharp fine structure features observed in the MIR spectra of crystalline silicates are completely absent in the spectra of synthetic silicate glasses. This is because silicate glasses lack the long-range order that gives rise to symmetry and anisotropy in crystals.

We constructed a calibration curve that can enable an investigator to derive the degree of polymerization of an amorphous silicate by using the Raman band area ratios $A_{(LF + MF)}/A_{(HF)}$—a calibration curve that exhibits a linear relationship with ln(NBO/T). This calibration curve was validated by using four natural silicate glasses, two terrestrial, and two extraterrestrial in origin, with more complicated chemistries. The results of this study suggest that, at least, semiquantification of the degree of polymerization of amorphous silicates in extraterrestrial materials can be achieved by using the Raman spectra acquired during future robotic planetary surface exploration missions.

Acknowledgments
All of the data used in this study can be found within the contents of this manuscript or in Tables S1–S7. This work of X.H. Fu was partially supported by the National Natural Science Foundation of China (grants 41303051, 41490633, and 41590851) and by the China Scholarship Council, which supported his visit to Washington University in St. Louis. A. Wang thanks a special financial support of the McDonnell Center for Space Sciences at Washington University in St. Louis for maintaining the collaboration with our Chinese colleagues. We thank David Gombosi (Syracuse University) for kindly providing Raman spectral data of the Apollo 16 glass beads.

References

Agee, C. B., et al. (2013), Unique meteorite from Early Amazonian Mars: Water-rich basaltic breccia Northwest Africa 7034, *Science*, *339*, 780–785.
Alberto, H., N. Ayres de Campos, and B. Mysen (1995), The structural role of titanium in silicate glasses: A Raman study of the system CaO–SiO_2–TiO_2, *Phys. Chem. Glasses*, *36*(3), 114–122.
Arredondo, E. H., and G. Rossman (2002), Feasibility of determining the quantitative OH content of garnets with Raman spectroscopy, *Am. Mineral.*, *87*, 307–311.
Baert, K., W. Meulebroeck, H. Wouters, A. Ceglia, K. Nys, H. Thienspont, and H. Terryn (2011), Using Raman spectroscopy as a tool for the detection of iron in glass, *J. Raman Spectrosc.*, *42*, 1789–1795.
Baker, L. L., and D. G. Strawn (2014), Temperature effects on the crystallinity of synthetic nontronite and implications for nontronite formation in Columbia River basalts, *Clays Clay Miner.*, *62*(2), 89–101.
Behrens, H., J. Roux, D. R. Neuville, and M. Siemann (2006), Quantification of dissolved H_2O in silicate glasses using confocal microRaman spectroscopy, *Chem. Geol.*, *229*(1–3), 96–112.
Bibring, J.-P., et al. (2007), Coupled ferric oxides and sulfates on the Martian surface, *Science*, *317*(5842), 1206–1210.
Bish, D. L., D. Blake, D. Vaniman, S. Chipera, R. Morris, D. Ming, A. Treiman, P. Sarrazin, S. Morrison, and R. T. Downs (2013), X-ray diffraction results from Mars Science Laboratory: Mineralogy of Rocknest at Gale Crater, *Science*, *341*(6153), 1238932.
Bishop, J. L., et al. (2008), Phyllosilicate diversity and past aqueous activity revealed at Mawrth Vallis, Mars, *Science*, *321*(5890), 830–833.
Brawer, S. A., and W. B. White (1975), Raman spectroscopic investigation of the structure of silicate glasses. I. The binary alkali silicates, *J. Chem. Phys.*, *63*(6), 2421–2432.
Brawer, S. A., and W. B. White (1977), Raman spectroscopic investigation of the structure of silicate glasses II. Soda-alkaline Earth-Alumina ternary and quaternary glasses, *J. Non Cryst. Solids*, *23*(2), 261–278.
Brearley, A. J., and C. Le Guillou (2015), More evidence of the importance of amorphous silicates in CM carbonaceous chondrites: New observations from a fine-grained rim in the CM2 chondrite, TIL 91722, in 78th Annual Meeting of the Meteoritical Society, edited, p. 5192.
Burns, R. G. (1993), Rates and mechanisms of chemical weathering of ferromagnesian silicate minerals on Mars, *Geochim. Cosmochim. Acta*, *57*(19), 4555–4574.
Cannon, K. M., and J. F. Mustard (2015), Preserved glass-rich impactites on Mars, *Geology*, doi:10.1130/G36953.1.
Changela, H. G., and J. C. Bridges (2010), Alteration assemblages in the nakhlites: Variation with depth on Mars, *Meteorit. Planet. Sci.*, *45*(12), 1847–1867.
Cooney, T. F., E. R. D. Scott, A. N. Krot, S. K. Sharma, and A. Yamaguchi (1999), Vibrational spectroscopic study of minerals in the Martian meteorite ALH 84001, *Am. Mineral.*, *84*(10), 1569–1576.
Dalby, K. N., and P. King (2006), A new approach to determine and quantify structural units in silicate glasses using micro-reflectance Fourier-transform infrared spectroscopy, *Am. Mineral.*, *91*, 1783–1793.

Daniel, I., P. Gillet, and P. Richet (1995), An in-situ high-temperature of stable and metastable polymorphs, *Mineral. Mag.*, *59*, 25–33.
Di Genova, D., D. Morgavi, K. U. Hess, D. R. Neuville, N. Borovkov, D. Perugini, and D. B. Dingwell (2015), Approximate chemical analysis of volcanic glasses using Raman spectroscopy, *J. Raman Spectrosc.*, *46*, 1235–1244.
Di Genova, D., K.-U. Hess, M. Oryaëlle Chevrel, and D. B. Dingwell (2016a), Models for the estimation of Fe^{3+}/Fe_{tot} ratio in terrestrial and extraterrestrial alkali-and iron-rich silicate glasses using Raman spectroscopy, *Am. Mineral.*, *101*(4), 943–952.
Di Genova, D., S. Kolzenburg, A. Vona, M. O. Chevrel, K.-U. Hess, D. R. Neuville, W. Ertel-Ingrisch, C. Romano, and D. B. Dingwell (2016b), Raman spectra of Martian glass analogues: A tool to approximate their chemical composition, *J. Geophys. Res. Planets*, *121*, 740–752, doi:10.1002/2016JE005010.
Di Muro, A., D. Giordano, B. Villemant, G. Montagnac, B. Scaillet, and C. Romano (2006), Influence of composition and thermal history of volcanic glasses on water content as determined by micro-Raman spectrometry, *Appl. Geochem.*, *21*(5), 802–812.
Di Muro, A., N. Métrich, M. Mercier, D. Giordano, D. Massare, and G. Montagnac (2009), Micro-Raman determination of iron redox state in dry natural glasses: Application to peralkaline rhyolites and basalts, *Chem. Geol.*, *259*(1–2), 78–88.
Etchepare, J. (1972), Study by Raman spectroscopy of crystalline and glassy diopside, *Amorphous Mater.*, 337–346.
Freeman, J. J., A. L. Wang, K. E. Kuebler, and L. A. Haskin (2008), Characterization of natural feldspar by Raman spectroscopy for future planetary exploration, *Can. Mineral.*, *46*(6), 1477–1500.
Furukawa, T., and W. B. White (1991), Raman spectroscopic investigation of the structure of silicate glasses. IV. Alkali-silico-germanate glasses, *J. Chem. Phys.*, *95*(2), 776–784.
Furukawa, T., K. E. Fox, and W. B. White (1981), Raman spectroscopic investigation of the structure of silicate glasses. III. Raman intensities and structural units in sodium silicate glasses, *J. Chem. Phys.*, *75*(7), 3226–3237.
Gombosi, D. J. (2013), Argon and neon diffusion in lunar impact glass & the development of the electron microprobe zircon fission-track dating technique, Syracuse Univ.
Greenberger, R., J. Mustard, P. Kumar, M. Dyar, E. Breves, and E. Sklute (2012), Low temperature aqueous alteration of basalt: Mineral assemblages of Deccan basalts and implications for Mars, *J. Geophys. Res.*, *117*, E00J12, doi:10.1029/2012JE004127.
Grotzinger, J. P., J. A. Crisp, and A. R. Vasavada (2015), Curiosity's mission of exploration at Gale Crater, Mars, *Elements*, *11*(1), 19–26.
Henderson, G. S. (2005), The structure of silicate melts: A glass perspective, *Can. Mineral.*, *43*(6), 1921–1958.
Hicks, L. J., J. C. Bridges, and S. J. Gurman (2014), Ferric saponite and serpentine in the nakhlite Martian meteorites, *Geochim. Cosmochim. Acta*, *136*, 194–210.
Horgan, B., and J. F. Bell III (2012), Widespread weathered glass on the surface of Mars, *Geology*, *40*(5), 391–394.
Huertas, F. J., S. Fiore, F. Huertas, and J. Linares (1999), Experimental study of the hydrothermal formation of kaolinite, *Chem. Geol.*, *156*(1–4), 171–190.
Izawa, M. R., R. L. Flemming, P. L. King, R. C. Peterson, and P. J. McCausland (2010), Mineralogical and spectroscopic investigation of the Tagish Lake carbonaceous chondrite by X-ray diffraction and infrared reflectance spectroscopy, *Meteorit. Planet. Sci.*, *45*(4), 675–698.
King, P., P. McMillan, and G. Moore (2004), Infrared spectroscopy of silicate glasses with application to natural systems, in *Molecules to Planets: Infrared Spectroscopy in Geochemistry, Exploration Geochemistry and Remote Sensing*, vol. 33, edited by P. L. King, pp. 93–133, Mineral Association of Canada, Ottawa.
Klein, C., C. S. Hurlbut, and J. D. Dana (2002), *The 22nd Edition of the Manual of Mineral Science: (After James D. Dana)*, Chichester, Wiley, New York.
Lange, R. A., and I. S. E. Carmichael (1989), Ferric-ferrous equilibria in Na_2O–FeO–Fe_2O_3–SiO_2 melts: Effects of analytical techniques on derived partial molar volumes, *Geochim. Cosmochim. Acta*, *53*(9), 2195–2204.
Launer, P. J. (1952), Regularities in the infrared absorption spectra of silicate minerals, *Am. Mineral.*, *37*(9–10), 764–784.
Leroux, H., and P. Cordier (2006), Magmatic cristobalite and quartz in the NWA 856 Martian meteorite, *Meteorit. Planet. Sci.*, *41*(6), 913–923.
Ling, Z. C., and A. L. Wang (2015), Spatial distributions of secondary minerals in the Martian meteorite MIL 03,346,168 determined by Raman spectroscopic imaging, *J. Geophys. Res. Planets*, *120*, 1141–1159, doi:10.1002/2015JE004805.
Long, D. A. (1977), *Raman Spectroscopy*, pp. 1–275, McGraw-Hill, New York.
Magnien, V., D. Neuville, L. Cormier, J. Roux, J.-L. Hazemann, O. Pinet, and P. Richet (2006), Kinetics of iron redox reactions in silicate liquids: A high-temperature X-ray absorption and Raman spectroscopy study, *J. Nucl. Mater.*, *352*(1), 190–195.
Marinov, M., N. Zotov, B. Mihailova, J. Nikolov, and L. Konstantinov (1994), The effect of disorder on the Raman spectra of glasses, *J. Phys. Condens. Matter*, *6*(20), 3813.
Matson, D. W., S. K. Sharma, and J. A. Philpotts (1983), The structure of high-silica alkali-silicate glasses. A Raman spectroscopic investigation, *J. Non Cryst. Solids*, *58*(2-3), 323–352.
McKeown, D. A. (2005), Raman spectroscopy and vibrational analyses of albite: From 25°C through the melting temperature, *Am. Mineral.*, *90*(10), 1506–1517.
McKeown, D. A., F. Galeener, and G. Brown (1984), Raman studies of Al coordination in silica-rich sodium aluminosilicate glasses and some related minerals, *J. Non Cryst. Solids*, *68*(2), 361–378.
McMillan, P. (1984a), A Raman spectroscopic study of glasses in the system CaO–MgO–SiO_2, *Am. Mineral.*, *69*, 645–659.
McMillan, P. (1984b), Structural studies of silicate glasses and melts: Applications and limitations of Raman spectroscopy? *Am. Mineral.*, *69*(7–8), 622–644.
McMillan, P., and B. Piriou (1983), Raman spectroscopic studies of silicate and related glass structure: A review, *Bull. Mineral.*, *106*(1–2), 57–75.
McMillan, P., B. Piriou, and A. Navrotsky (1982), A Raman spectroscopic study of glasses along the joins silica-calcium aluminate, silica-sodium aluminate, and silica-potassium aluminate, *Geochim. Cosmochim. Acta*, *46*(11), 2021–2037.
McMillan, P., S. Jakobsson, J. R. Holloway, and L. A. Silver (1983), A note on the Raman spectra of water-bearing albite glasses, *Geochim. Cosmochim. Acta*, *47*(11), 1937–1943.
McSween, H. Y. (2015), Petrology on Mars, *Am. Mineral.*, *100*(11-12), 2380–2395.
Mercier, M., A. Di Muro, D. Giordano, N. Métrich, P. Lesne, M. Pichavant, B. Scaillet, R. Clocchiatti, and G. Montagnac (2009), Influence of glass polymerisation and oxidation on micro-Raman water analysis in alumino-silicate glasses, *Geochim. Cosmochim. Acta*, *73*(1), 197–217.
Merzbacher, C. I., and W. B. White (1991), The structure of alkaline earth aluminosilicate glasses as determined by vibrational spectroscopy, *J. Non Cryst. Solids*, *130*(1), 18–34.
Moroz, L. V., et al. (2009), Spectral properties of simulated impact glasses produced from Martian soil analogue JSC Mars-1, *Icarus*, *202*(1), 336–353.
Mustard, J. F., et al. (2008), Hydrated silicate minerals on Mars observed by the Mars Reconnaissance Orbiter CRISM instrument, *Nature*, *454*(7202), 305–309.
Mysen, B., and D. Neuville (1995), Effect of temperature and TiO_2 content on the structure of Na_2Si_2O5-$Na_2Ti_2O_5$ melts and glasses, *Geochim. Cosmochim. Acta*, *59*(2), 325–342.

Mysen, B. O. (2003), Physics and chemistry of silicate glasses and melts, *Eur. J. Mineral.*, *15*(5), 781–802.
Mysen, B. O., and M. J. Toplis (2007), Structural behavior of Al^{3+} in peralkaline, metaluminous, and peraluminous silicate melts and glasses at ambient pressure, *Am. Mineral.*, *92*(5–6), 933–946.
Mysen, B. O., and P. Richet (2005), *Silicate Glasses and Melts: Properties and Structure*, Elsevier, Amsterdam.
Mysen, B. O., F. Seifert, and D. Virgo (1980a), Structure and redox equilibria of iron-bearing silicate melts, *Am. Mineral.*, *65*(9–10), 867–884.
Mysen, B. O., D. Virgo, and C. M. Scarfe (1980b), Relations between the anionic structure and viscosity of silicate melts; a Raman spectroscopic study, *Am. Mineral.*, *65*(7–8), 690–710.
Mysen, B. O., D. Virgo, and I. Kushiro (1981), The structural role of aluminum in silicate melts; a Raman spectroscopic study at 1 atmosphere, *Am. Mineral.*, *66*(7–8), 678–701.
Mysen, B. O., D. Virgo, and F. A. Seifert (1982), The structure of silicate melts: Implications for chemical and physical properties of natural magma, *Rev. Geophys.*, *20*(3), 353–383, doi:10.1029/RG020i003p00353.
Neuville, D. R., and B. O. Mysen (1996), Role of aluminium in the silicate network: In situ, high-temperature study of glasses and melts on the join SiO_2–$NaAlO_2$, *Geochim. Cosmochim. Acta*, *60*(10), 1727–1737.
Neuville, D. R., D. de Ligny, and G. S. Henderson (2014), Advances in Raman spectroscopy applied to earth and material sciences, *Rev. Mineral. Geochem.*, *78*(1), 509–541.
Noguchi, T., T. Nakamura, and W. Nozaki (2002), Mineralogy of phyllosilicate-rich micrometeorites and comparison with Tagish Lake and Sayama meteorites, *Earth Planet. Sci. Lett.*, *202*(2), 229–246.
Osinski, G. R., L. L. Tornabene, and R. A. Grieve (2011), Impact ejecta emplacement on terrestrial planets, *Earth Planet. Sci. Lett.*, *310*(3), 167–181.
Piriou, B. (1983), The high-frequency vibrational spectra of vitreous and crystalline orthosilicates, *Am. Mineral.*, *68*, 426–443.
Poulet, F., J. P. Bibring, J. F. Mustard, A. Gendrin, N. Mangold, Y. Langevin, R. E. Arvidson, B. Gondet, and C. Gomez (2005), Phyllosilicates on Mars and implications for early martian climate, *Nature*, *438*(7068), 623–627.
Rampe, E., R. Morris, S. Ruff, B. Horgan, E. Dehouck, C. Achilles, D. Ming, D. Bish, and S. Chipera (2014), Amorphous phases on the surface of Mars.
Rossano, S., and B. Mysen (2012), Raman spectroscopy of silicate glasses and melts in geological systems, *EMU Notes Miner.*, *12*.
Rull, F., and the RSL team (2014), The laser Raman instrument (RLS) for EXOMARS 2018 mission and the scientific operation on Mars. LPI Contributions, 1791, p.1277.
Salisbury, J. W., and A. Wald (1992), The role of volume scattering in reducing spectral contrast of reststrahlen bands in spectra of powdered minerals, *Icarus*, *96*(1), 121–128.
Salisbury, J. W., D. M. D'Aria, and E. Jarosewich (1991), Midinfrared (2.5–13.5 μm) reflectance spectra of powdered stony meteorites, *Icarus*, *92*(2), 280–297.
Seifert, F. A., B. O. Mysen, and D. Virgo (1981), Structural similarity of glasses and melts relevant to petrological processes, *Geochim. Cosmochim. Acta*, *45*(10), 1879–1884.
Sharma, S. K., and B. Simons (1981), Raman study of crystalline polymorphs and glasses of spodumene composition quenched from various pressures, *Am. Mineral.*, *66*(1–2), 118–126.
Sharma, S. K., and D. W. Matson (1984), Raman spectra and structure of sodium aluminogermanate glasses, *J. Non Cryst. Solids*, *69*(1), 81–96.
Sharma, S. K., T. F. Cooney, Z. Wang, and S. van der Laan (1997), Raman band assignments of silicate and germanate glasses using high-pressure and high-temperature spectral data, *J. Raman Spectrosc.*, *28*(9), 697–709.
Skok, J., J. Mustard, L. Tornabene, C. Pan, D. Rogers, and S. Murchie (2012), A spectroscopic analysis of Martian crater central peaks: Formation of the ancient crust, *J. Geophys. Res.*, *117*, E00J18, doi:10.1029/2012JE004148.
Speck, A. K., A. G. Whittington, and A. M. Hofmeister (2011), Disordered silicates in space: A study of laboratory spectra of "amorphous" silicates, *Astrophys. J.*, *740*(2), 93.
Thomas, R. (2000), Determination of water contents of granite melt inclusions by confocal laser Raman microprobe spectroscopy, *Am. Mineral.*, *85*, 868–872.
Thomas, S. M., R. Thomas, P. Davidson, P. Reichart, M. Koch-Muller, and G. Dollinger (2008), Application of Raman spectroscopy to quantify trace water concentration in glasses and garnets, *Am. Mineral.*, *93*, 1550–1557.
Tornabene, L., A. McEwen, C. Caudill, G. Osinski, J. Wray, G. Marzo, J. Mustard, J. Skok, J. Grant, and S. Mattson (2010), A crater-exposed bedrock database for Mars with applications for determining the composition and structure of the upper crust, paper presented at Lunar and Planet. Sci. Conf.
Vaniman, D., D. Bish, D. Ming, T. Bristow, R. Morris, D. Blake, S. Chipera, S. Morrison, A. Treiman, and E. Rampe (2014), Mineralogy of a mudstone at Yellowknife Bay, Gale Crater, Mars, *Science*, *343*(6169), 1243480.
Virgo, D., B. Mysen, and I. Kushiro (1980), Anionic constitution of 1-atmosphere silicate melts: Implications for the structure of igneous melts, *Science*, *208*(4450), 1371–1373.
Wang, A., and B. Jolliff (2015), Phyllosilicate-like species in Tagish Lake meteorite as seen by Raman spectroscopy, paper presented at Lunar and Planet. Sci. Conf.
Wang, A., B. L. Jolliff, and L. A. Haskin (1995), Raman spectroscopy as a method for mineral identification on lunar robotic exploration missions, *J. Geophys. Res.*, *100*(E10), 21,189–21,199, doi:10.1029/95JE02133.
Wang, A., B. L. Jolliff, L. A. Haskin, K. E. Kuebler, and K. M. Viskupic (2001), Characterization and comparison of structural and compositional features of planetary quadrilateral pyroxenes by Raman spectroscopy, *Am. Mineral.*, *86*(7–8), 790–806.
Wang, A., R. L. Korotev, B. L. Jolliff, and Z. Ling (2015), Raman imaging of extraterrestrial materials, *Planet. Space Sci.*, *112*, 23–34.
Wang, Z., T. F. Cooney, and S. K. Sharma (1995), In situ structural investigation of iron-containing silicate liquids and glasses, *Geochim. Cosmochim. Acta*, *59*(8), 1571–1577.
Wiens, R. C., et al. (2016), The SuperCam remote sensing instrument suite for Mars 2020, in 47th Lunar and Planet. Sci. Conf., p. 1322.
Williams, Q., P. McMillan, and T. F. Cooney (1989), Vibrational spectra of olivine composition glasses: The Mg–Mn join, *Phys. Chem. Miner.*, *16*(4), 352–359.
Zajacz, Z., et al. (2005), A composition-independent quantitative determination of the water content in silicate glasses and silicate melt inclusions by confocal Raman spectroscopy, *Contrib. Mineral. Petrol.*, *150*, 631–642.
Zolensky, M., K. Nakamura, M. Gounelle, T. Mikouchi, T. Kasama, O. Tachikawa, and E. Tonui (2002), Mineralogy of Tagish Lake: An ungrouped type 2 carbonaceous chondrite, *Meteorit. Planet. Sci.*, *37*(5), 737–761.
Zotov, N., H. Keppler, A. Hannon, and A. Soper (1996), The effect of water on the structure of silicate glasses—A neutron diffraction study, *J. Non Cryst. Solids*, *202*(1), 153–163.
Zotov, N., I. Ebbsjö, D. Timpel, and H. Keppler (1999), Calculation of Raman spectra and vibrational properties of silicate glasses: Comparison between Na2Si4O9 and SiO2 glasses, *Phys. Rev. B*, *60*(9), 6383.